Ionic Liquid *Versus* Prodrug Strategy to Address Formulation Challenges

Anja Balk • Toni Widmer • Johannes Wiest • Heike Bruhn • Jens-Christoph Rybak • Philipp Matthes • Klaus Müller-Buschbaum • Anastasios Sakalis • Tessa Lühmann • Jörg Berghausen • Ulrike Holzgrabe • Bruno Galli • Lorenz Meinel

ABSTRACT

Purpose A poorly water soluble acidic active pharmaceutical ingredient (API) was transformed into an ionic liquid (IL) aiming at faster and higher oral availability in comparison to a prodrug.

Methods API preparations were characterized in solid state by single crystal and powder diffraction, NMR, DSC, IR and in solution by NMR and ESI-MS. Dissolution and precipitation kinetics were detailed as was the role of the counterion on API supersaturation. Transepithelial API transport through Caco-2 monolayers and counterion cytotoxicity were assessed.

Results The mechanism leading to a 700 fold faster dissolution rate and longer duration of API supersaturation of the ionic liquid in comparison to the free acid was deciphered. Transepithelial transport was about three times higher for the IL in comparison to the prodrug when substances were applied as suspensions with the higher solubility of the IL outpacing the higher permeability of the prodrug. The counterion was nontoxic with IC_{50} values in the upper μM / lower mM range in cell lines of hepatic and renal origin as well as in macrophages.

Conclusion The IL approach was instrumental for tuning physico-chemical API properties, while avoiding the inherent need for structural changes as required for prodrugs.

Anja Balk and Toni Widmer are the first two authors should be regarded as joint first authors

A. Balk • T. Widmer • J. Wiest • J.-C. Rybak • A. Sakalis • T. Lühmann • U. Holzgrabe • L. Meinel (✉)
Institute for Pharmacy, Am Hubland, University of Würzburg, 97074 Würzburg, Germany
e-mail: l.meinel@pharmazie.uni-wuerzburg.de

T. Widmer • J. Berghausen • B. Galli
Novartis Pharma AG, Lichtstraße 35 4002 Basel, Switzerland

H. Bruhn
Institute for Molecular Infection Biology, Josef-Schneider-Straße 2 97080 Würzburg, Germany

P. Matthes • K. Müller-Buschbaum
Institute of Inorganic Chemistry, Am Hubland, University of Würzburg, 97074 Würzburg, Germany

INTRODUCTION

Improper solubility jeopardizes biopharmaceutical impact of pharmaceuticals and ultimately delays relief to the suffering. This problem is aggravated in pharmaceutics today as a result of high throughput screening (HTS) based research strategies for lead identification. By HTS preferentially lipophilic and high molecular weight molecules are selected, posing an additional developmental challenge, for these molecules are typically less soluble in water [1, 2]. To overcome the low bioavailability, the concept of transforming an active pharmaceutical ingredient (API) into an ionic liquid (IL) is presented in this manuscript. ILs are organic salts with a melting point below 100°C and are dissociated to some extent into ions [3, 4] and have been developed to address e.g. solubility challenges [5]. Another improvement of permeability and / or solubility may be by converting a parent drug into a prodrug [6]. The prodrug concept is well established, however, challenging from a drug regulatory perspective as it constitutes a new API.

We compared the IL strategy to a prodrug concept with the aim to improve the biopharmaceutical properties of a new, orally active α-amino-3-hydroxy-5-methyl-4-isoxazolepropionic acid receptor (AMPA) antagonist [7–9], which was administered to patients with acute migraine attacks at a dose of 250 mg before [10]. We identified the physical-chemical mechanism to achieve improved biopharmaceutical properties of the IL in comparison to the free acid,

its potassium salt, and an acetylated prodrug. These interpretations were based on structural information collected in the solid (single crystal, NMR, DSC) and liquid state (NMR), including a precise characterization of ion pairing (NMR, ESI-MS), solubility patterns (acid–base titration experiments), dissolution and precipitation kinetics at the supersaturated and equilibrium phase, respectively. Counterion toxicity was tested in three cell lines of hepatic and renal origin and in macrophages [11]. Data sets from the physical-chemical characterization were correlated to transport kinetics through relevant jejunal *in vitro* model system.

RESULTS

Structure and Physical Characteristics

The structural formula of N-[7-isopropyl-6-(2-methyl-2H-pyrazol-3-yl)-2,4-dioxo-1,4-dihydro-2*H*-quinazolin-3-yl]-methanesulfonamide (referred to as 'free acid') and its prodrug (acetylated at the methylenesulfonamido group; referred to as 'prodrug') are provided (Fig. 1(a); formula of the counterion tetrabutylphosphonium is not shown). The free acid crystallized in an orthorhombic space group (*Pbca*) and molecules
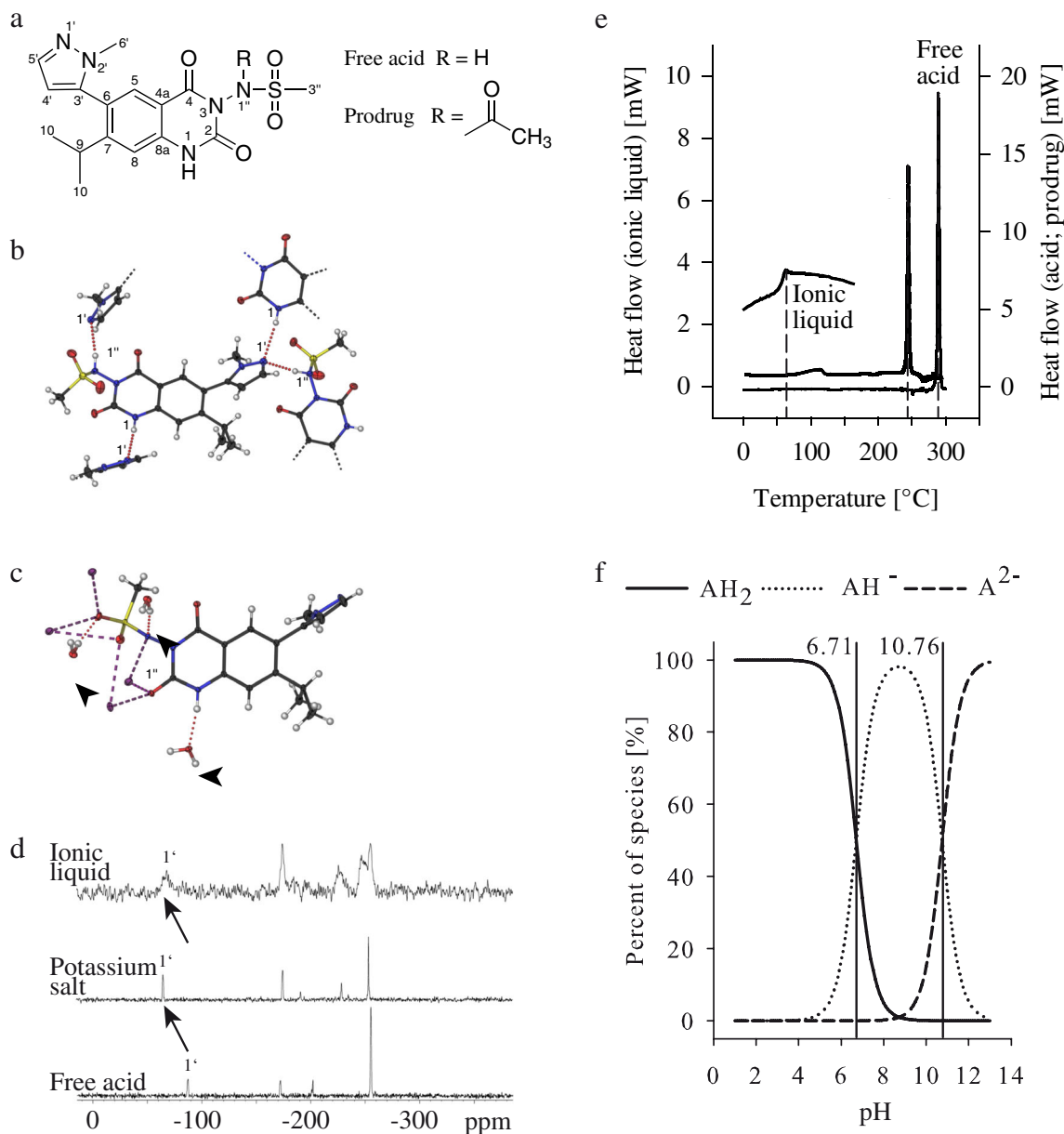

Fig. 1 (**a**) Structural formula of the free acid and the prodrug. Crystal structure of the (**b**) free acid and (**c**) the potassium salt of the free acid (a monohydrate) and as determined by single crystal diffractometry. Crystal water is highlighted by arrowheads and the interaction of the potassium cation with the acid is illustrated by dashed rods. (**d**) Solid state ^{15}N NMR spectra displaying the high field shift of the N-1′ signal of the ionic liquid and the potassium salt in comparison to the free acid. (**e**) Glass transition temperature (ionic liquid) and melting points of the prodrug and the free acid, respectively, and as determined by dynamic scanning calorimetry. (**f**) Distribution of species as a function of pH as determined potentiometrically.

were arranged in layers (Fig. 1(b); Supplementary Figure 1A). Within each layer, one molecule was connected to four neighboring molecules via hydrogen bonds. In particular, the unsubstituted nitrogen atom of the pyrazole ring interacted with the hydrogen atom in the sulfonamide group and the hydrogen atom at the unsubstituted nitrogen atom in the 2,4-quinazolindione ring (Fig. 1(b); Supplementary Figure 1A; Table I). The potassium salt crystallized as a monohydrate in the monoclinic space group $P2_1/c$ (Fig. 1(c), Table I). In this crystal structure, potassium ions (K^+-ions) formed layers in the crystallographic *bc*-plane with the acid anions placed atop and below the K^+ ions (Supplementary Figure 1B). The atomic distances between K^+-ions and nitrogen and oxygen atoms (Supplementary Figure 1B, Table I) suggested ionic interactions between the K^+-ion and four partners, (i) the oxygen atoms and the (ii) nitrogen atom of the sulfonamide group as well as to (iii) one oxygen atom of the quinazolindione ring and to (iv) one crystal water molecule, respectively (Fig. 1(c), Supplementary Figure 1B). In contrast to the crystal structure of the free acid, no direct hydrogen bonds were observed between the organic molecules (Fig. 1(c), Supplementary Figure 1B). The free acid, its potassium salt and the prodrug were crystalline whereas the IL was amorphous as determined by XRPD (Supplementary Figure 2A) and no birefringence was observed by polarized light microscopy (data not shown). Solid state ^{15}N NMR spectra were recorded for all three forms, the IL, the free acid and the potassium salt (see Fig. 1(d)). The nitrogen signals were assigned by long-range ^1H-^{15}N HMBC, HSQC and INEPT experiments in solution at room temperature and −70°C (data not shown) with the N-1′ to δ at −87.2 ppm and N-2′ to δ at −172.1 ppm, respectively. Interestingly, the N-1′ signal was shifted to δ = −64.1 ppm in the spectrum of the IL and to δ = −64.8 ppm in the potassium salt. In the IR spectrum of the free acid, characteristic stretching vibrations were observed at 3146 cm^{-1} for the N-H (1″), and for the sulfonamide group at 1343 and 1150 cm^{-1}, respectively. For the potassium salt no stretching vibration of N-H (1″) at 3146 cm^{-1} was detected and the

absorption band was shifted to 1247 and 1107 cm^{-1} indicating the deprotonation of the API. In analogy to the observations for the potassium salt, the IL produced no signal of N-H (1″) at 3146 cm^{-1} and the stretching vibration for the sulfonamide group was shifted to 1243 and 1104 cm^{-1} (Supplementary Figure 2C). The melting point for the prodrug and the free acid were read from endothermic peak 244 and 290°C, respectively, and the glass transition temperature of the IL was observed at about 57°C (Fig. 1(e)). A broad endothermic peak with an onset at 150°C and a concomitant mass loss of about 4% was observed for the potassium salt (monohydrate), indicating the loss of hydrate water at that temperature (corresponding TGA data Supplementary Figure 2B). No melting was detected before degradation onset at about 275°C. Two pKa values were found for the free acid at 6.7 and 10.8 (Fig. 1(f)) linked to the N-1″ (6.7; as a result of a high-field shift of the methyl group of the methylenesulfonamide group in the ^1H NMR spectrum observed at pH 7.6) and to the nitrogen in position 1 of the quinazolinedione ring (10.8; as a result of the high-field signal shift of the aromatic hydrogen H-8 and to a lesser extent of H-5 observed at pH 11.75) (Supplementary Figure 3A, Supplementary Figure 3C). After storage of the IL for 18 month *in vacuo* no crystallinity was detected by XRPD (date not shown). Furthermore, no changes in ^1H NMR spectrum were observed and the glass transition temperature was unaltered (data not shown) as compared to baseline.

Dissolution Rate, Duration of Supersaturation, Solubility, Precipitation Rate and Formation of Supramolecular Aggregates

Drug substance dissolution rate in PBS buffer pH 6.8 was more than 700 fold higher for the IL, as compared to the free acid and twice as high as compared to the potassium salt (Fig. 2). The dissolution rate of the free acid was not different as compared to the blend of the free acid with tetrabutylphosphonium added to the dissolution medium.

Table I Single crystal X-ray data of the free acid and the potassium salt, respectively

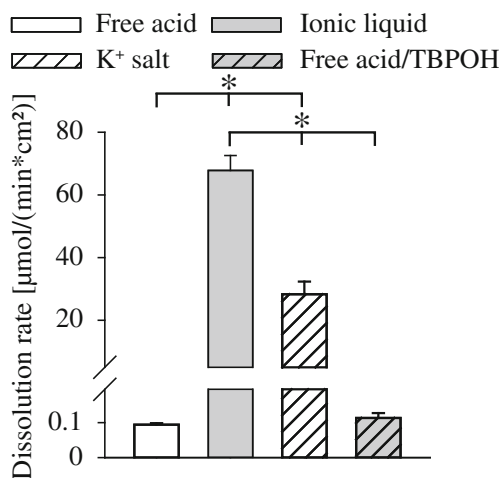| Crystal system Space group	Free acid ($C_{16}H_{19}N_5O_4S$) $M_r = 377.43$ orthorhombic Pbca	K^+ salt ($C_{16}H_{20}N_5O_5SKCl$) $M_r = 433.53$ monoclinic $P2_1/c$
a [Å]	15.0318 (10)	22.8265 (6)
b [Å]	12.0212 (8)	5.8993 (2)
c [Å]	19.5095 (13)	15.3597 (4)
α [°]	90	90.00
β [°]	90	104.2530 (10)
γ [°]	90	90.00
Volume [Å^3]	3525.4 (4)	2004.67 (10)
Z value	8	4
D$_{calc}$ [g/cm^3]	1.4221	1.436

Fig. 2 Dissolution rate of the bulk qualities of the free acid, ionic liquid, potassium salt and an equimolar blend of the free acid and the counterion in dissolution medium.

The duration of supersaturation, calculated from the concentration *versus* time profiles determined by potentiometric titration [12], was for the free acid (10 ± 2 min) < potassium salt (12 ± 1 min) < blend of the free acid and the counterion (22 ± 6 min) < IL (35 ± 15 min) (Fig. 3(a), (b)). The duration observed for the IL and the blend (free acid and counterion) was significantly longer as compared to the free acid and its potassium salt ($p < 0.05$). The duration of supersaturation was further measured by real-time precipitation experiments, complementing these accelerated potentiometric titrations (Fig. 3(c), (d)). In these, the IL did not demonstrate a pH shift with the solution remaining clear throughout 12 h (end of experiment). In contrast, a significant pH shift and precipitation was observed after about 12 min (± 1 min) for the potassium salt (Fig. 3(c), (d)). The dissolution rates for the IL or the free acid were comparable in acetate buffer (data not shown).

The peak concentration during the supersaturation phase (kinetic solubility), determined by potentiometric titration, was typically higher for the free acid or its potassium salt in

Fig. 3 API concentration [mM] – time [minutes] profile for the (**a**) free acid, ionic liquid, (**b**) potassium salt and an equimolar blend of the free acid and the counterion, respectively. Change in pH due to precipitation – time [h] profile of (**c**) potassium salt and (**d**) ionic liquid.
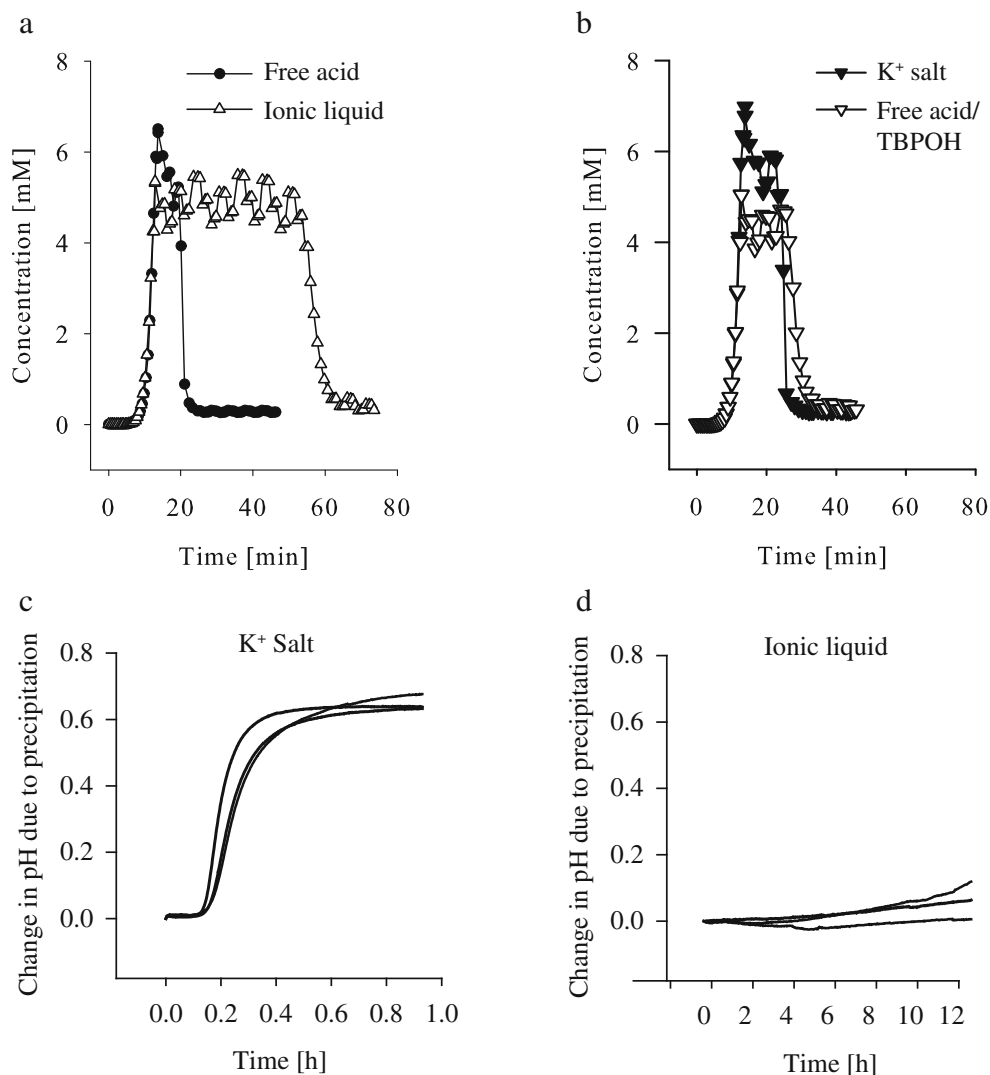
comparison to the IL or the blend of the free acid and the counterion (Figs. 3(a), (B) and 4(a)). The kinetic solubility recorded for the potassium salt was significantly higher as compared to all other groups ($p < 0.05$), followed by the free acid, which had a higher kinetic solubility as compared to the IL and the blend (free acid and counterion; $p < 0.05$) the latter two groups of which demonstrating equal kinetic solubility

(Fig. 4(a)). The intrinsic solubility (equilibrium solubility) was generally an order of magnitude lower as compared to the kinetic solubility for all groups (Fig. 4(b)). The ratio of the dissolution rate and the precipitation rate measured from the precipitates at supersaturation, was significantly higher for the IL in comparison to the free acid and the potassium salt ($p < 0.05$) and equal for the free acid and the potassium salt,

Fig. 4 (**a**) Kinetic solubility [mM] and (**b**) intrinsic solubility [mM] of the APIs and blend of free acid and *counterion*. (**c**) Ratio of the dissolution rate over the precipitation rate of the precipitate in the supersaturated phase (S) and at equilibrium (E) for the free acid, ionic liquid and the potassium salt, respectively. Asterisks indicate statistically significant differences among groups ($p < 0.05$). (**d**) Superimposition of expansions from NMR spectra of the supersaturated phase (S) and in the equilibrium phase (E). The signals of the terminal methyl group of the *counterion* (tetrabutylphosphonium) at δ ~ 0.85 ppm and H-5′ of the pyrazole ring at δ ~ 6.3–6.4 ppm are displayed. (**e**) Overview of the duration of the supersaturation phase [minutes] as a function of the ratio of kinetic solubility over equilibrium solubility (supersaturation ratio) for the free acid, the ionic liquid and different blends of the free acid and the *counterion*. (**f**) Duration of supersaturation [minutes] as a function of different blends of the free acid and the *counterion*.
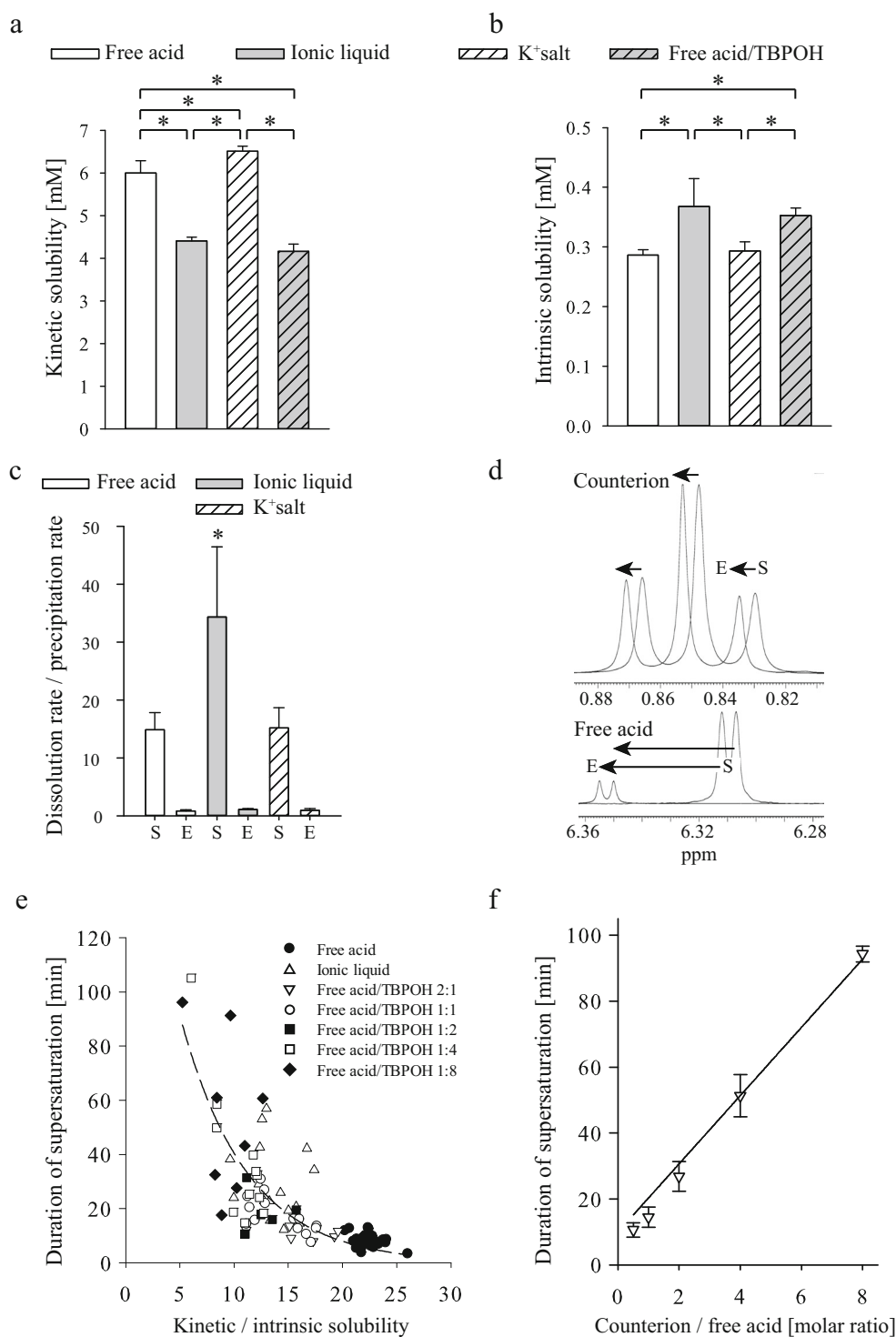
respectively (Fig. 4(c)). In contrast, no differences among groups were observed in the rates observed at equilibrium (Fig. 4(c)).

The IL was further characterized for the presence of soluble supramolecular aggregates when dissolved in water. At a concentration of 1 mM, the electrospray ionization mass spectrum (ESI-MS) in the positive ion mode revealed peaks corresponding to an aggregate formation following the general pattern of $[A_n]^-$ (with signals for n from 1 to 5) and $[A_nK]^-$ (with signals for n from 1 to 7; Supplementary Figure 3B) [13]. Lower API concentrations did not show these aggregates (data not shown). Analogous studies following dissolution of the free acid in 30 or 70% acetonitrile in water, respectively, exhibited an increasingly complex association pattern for the free acid as compared to pure water, following $[A_nK_o]^-$, with the index n being an integer between 1 and 6 and o between 1 and 4 for the 70% acetonitrile in water solution (data not shown). The supramolecular association of the API in solution was further analyzed by a ^{1}H NMR based aggregation assay [14] . The superimposition of the ^{1}H NMR spectra collected in the supersaturated and the equilibrium phase exhibited a clear high field shift of all signals in the supersaturated phase with the overall number of signals remaining constant (Fig. 4(d)). The signal intensity of the API was substantially reduced when comparing the supersaturated and the equilibrium phase and in comparison to those of the counterion, which was concluded by comparing the H-5′ signal of the pyrazole moiety and the terminal methyl group signal of the counterion, respectively (Fig. 4(d)). This suggested the precipitation of the IL as the free acid with the counterion remaining in solution.

The duration of supersaturation was exponentially related to supersaturation ratio, following a general trend as approximated by duration of supersaturation $= 206*e^{-0,16*S}$ ($r^2 = 0.62$), with S being the supersaturation ratio as calculated by dividing the kinetic by the equilibrium solubility, respectively (Fig. 4(e)). The duration of supersaturation was linearly correlated to the ratio of the counterion and the free acid by duration of supersaturation $= 10 + 10*$ ratio ($r^2 = 0.98$), with the ratio being the molar amount of the counterion divided by the amount of free acid (Fig. 4(f)).

Characterization of Precipitates in Supersaturated and Equilibrium State

Time lapsed diffractometric studies on precipitates collected from the supersaturated phase and the equilibrium phase analyzed under gradual drying, revealed different crystallization kinetics for the free acid and the IL (Fig. 5). The precipitate of the free acid was amorphous in the supersaturated phase and this state was maintained for up to 14 min throughout the continuous diffractometric monitoring (Fig. 5(a)). However, after 21 min the reflection of the potassium chloride

– as present from the solubility experiments which were conducted in presence of potassium chloride and from which the precipitates were collected – was observed at about 28° (Fig. 5(a)) along with reflections of the free acid (Supplementary Figure 2A). Similar to the free acid, the precipitate collected from the supersaturated phase of the IL displayed an amorphous structure at the beginning of the time-lapsed measurements (Fig. 5(b)). After 14 min, the potassium chloride reflection was observed at about 28°, with the IL still being in amorphous form – a state, which was maintained up to 42 min after which the experiment was stopped. In contrast, precipitates collected from the free acid and the IL collected in the equilibrium phase had identical reflections.

Furthermore, the precipitates were analyzed by ^{1}H NMR measurements. The precipitate of the IL collected from the supersaturated phase (dissolved in DMSO-d$_6$) was measured and the hydrogens attached to the N-1 and N-1″ showed one broad signal ($\delta = 10$–12.5 ppm; Fig. 5(c)) indicating a single deprotonation (assignment of deprotonation to N-1 and N-1″ was verified by EXSY experiments at room temperature and $-70°$C due to rapid proton exchange among groups). In contrast, two resonances were seen in the precipitate harvested from the equilibrium phase indicating that both groups, the N-1″ and the N-1 were protonated and supporting that precipitation occurred as the free acid (Fig. 5(c)) as both signals were also observed for the free acid in equilibrium state (Fig. 5(c)). The counterion was present in the precipitates collected from the supersaturated phase of the IL (Fig. 5(c), arrows; $\delta = 0.5$–4 ppm), with an estimated ratio of the API to the counterion of about 6 : 1 as calculated from the integrals of the ^{1}H NMR signals. In contrast, the precipitates harvested from the equilibrium phase showed only traces of the counterion and yielded almost identical spectra as obtained for the free acid (Fig. 5(c)). ^{1}H NMR measurements of the precipitate of the free acid collected from the supersaturated state displayed the same broad signal as observed for the IL (data not shown), however no tetrabutlyphosphonium signals were detected. After equilibrium state was reached precipitates displayed the same ^{1}H NMR spectra as the bulk substance.

In Vitro Permeability Through the Caco-2 Cell Monolayer Model

Caco-2 cell monolayers were characterized before use. All monolayers had TEER values of at least $600\Omega*$cm^2 and paracellular permeability and monolayer tightness was demonstrated by sodium fluorescein transport with mean P_{app} values $<10^{-7}$ cm/s (apical to basolateral; data not shown) [15]. Furthermore, the monolayers were morphologically characterized for the location and distribution of cell nuclei through DAPI stain (blue) and tight junctions were labeled by e-cadherin staining (Fig. 6(a)). In a first experiment, API were applied as *solutions* to the apical compartment, resulting in
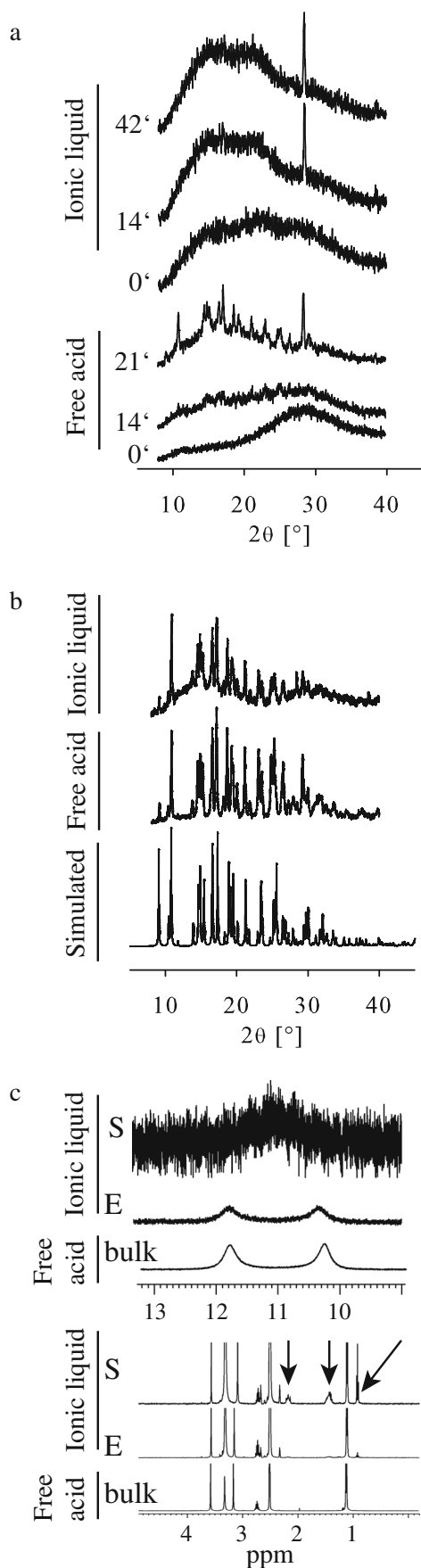
a

b

c

Fig. 5 Time lapsed powder diffractograms. Numbers within charts indicate the time [minutes] after the set of experiments commenced. Suspensions gradually dried under ambient conditions within the diffractometer and during measurement. Representative diffractograms of precipitates collected from the supersaturation phase of the (**a**) ionic liquid and the free acid. (**b**) Representative diffractograms of precipitates collected from the equilibrium phase of the ionic liquid and the free acid. A simulated diffractogram as calculated from the single crystal data of the free acid is provided. (**c**) ^{1}H NMR of the precipitates collected in the supersaturated phase (S) and in the equilibrium phase (E) for the free acid and the ionic liquid, respectively (precipitates were re-dissolved in DMSO after collection and right before measurement). Spectra of the bulk free acid are given for comparison (bulk). The upper set of three spectra shows the signal of the hydrogen bound to the methylenesulfonamide group (H-1″). The lower set of three spectra shows the region within which signals by the *counterion* are detected and as highlighted by the *arrowheads*.

comparable normalized molar amounts found basolaterally over time for the IL and the free acid while the amount of transported prodrug was significantly higher ($p < 0.05$; Fig. 6(b)). In a second experiment, a *suspension* of the API was used in the apical compartment instead of the API solution applied in the previous set-up (Fig. 6(c), (d)). The concentration in the apical chamber of the free acid was approximately three times higher than the concentration observed for the prodrug ($p < 0.05$) and four times lower than the concentration of the IL ($p < 0.05$; Fig. 6(c)). The molar API amounts analyzed within the basolateral compartment over time were significantly and typically five times higher for the IL as compared to the free acid or the prodrug (Fig. 6(d)).

Counterion Cytotoxicity

Cytotoxicity of tetrabutylphosphonium chloride was analyzed *in vitro* in three cell lines with an AlmarBlue based assay. IC_{50} values were 712 ± 14 µM for HepG2 cells, 248 ± 48 µM in HEK 293 T cells and >1000 µM for J774.1 cells.

DISCUSSION

We defined the IL based on the observed glass transition below 100°C (Fig. 1(e)) and the ionic nature determined by solid state ^{15}N NMR (Fig. 1(d)) and IR spectroscopy (Supplementary Figure 2C). For both the IL and the potassium salt, the N-1′ signal of the pyrazole nitrogen was shifted almost identically in contrast to the high field shift of this signal for the free acid (Fig. 1(d)). Crystal structure data detailed these findings to the deprotonation of the methylenesulfonamide group of the potassium salt (Fig. 1(c)). While the proton of the methylenesulfonamide group of the acid is part of a hydrogen bond to the pyrazole nitrogen N-1′, no such interaction is possible for the deprotonated potassium salt, resulting in a

Fig. 6 Transport studies through an *in vitro* Caco-2 cell culture model of the human small intestinal mucosa and grown on a cell culture insert filter. (**a**) Representative confocal microscopy image after immunohistological staining of cell-cell contacts (e-cadherin, green) and cell nuclei (DAPI, blue). *Bar* length = 20 μm. (**b**) Amount of API [nmol] as measured from samples taken from the basolateral chamber at different time points [minutes]. Solutions of the free acid, the ionic liquid and the prodrug were administered to the apical chamber, respectively. (**c**) Amounts of dissolved API when applied as suspension to the apical chamber for the free acid, the ionic liquid and the prodrug, respectively. (**d**) Amount of API [nmol] as measured from samples taken from the basolateral chamber at different time points [minutes]. Suspensions of the free acid, the ionic liquid and the prodrug were administered to the apical chamber, respectively. Asterisks indicate statistically significant differences among groups ($p < 0.05$).
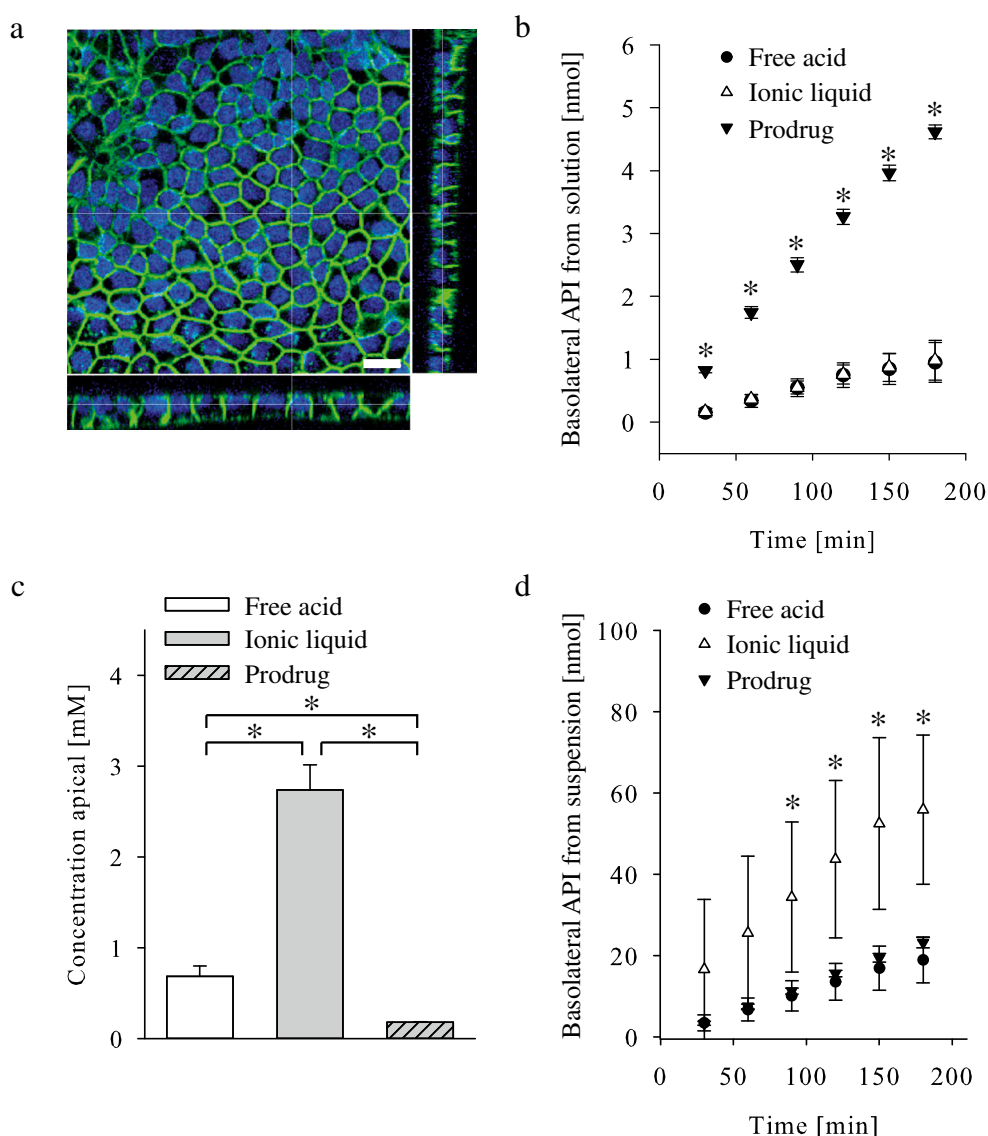
shifted N-1′ signal to higher field. In the IR spectra an identical shift of the methylenesulfonamide group after deprotonation for both the potassium salt and IL was observed (Supplementary Figure 2C). Therefore, the solid state ^{15}N NMR and IR spectroscopy data confirmed the ionic nature of the IL in solid state. Stored *in vacuo* the IL was stable for 18 month, with no recrystallization and no shift in glass transition temperatures occurring throughout the storage period, an important yet preliminary finding regarding drug substance stability. Further studies including stress tests are required to detail the stability under real life or accelerated conditions.

The drug substance dissolution rate of the IL exceeded the potassium salt and even more the free acid (Fig. 2). The faster dissolution of the IL and the potassium salt in comparison to the free acid is likely a result of the ionization whereas the differences of the (amorphous) IL in comparison to the (crystalline) potassium salt are attributed to the different lattice forces.

A prolonged supersaturation was observed for the IL (Fig. 3(a)). The observation for the IL matched the classical nucleation theory [16, 17], linking the rate of crystal formation $\mathcal{J}$ exponentially to the supersaturation ratio and given by $j = Ae\left(\frac{B}{\ln^2 S}\right)$. A and B are typically regarded as constants with $\frac{B}{\ln^2 S} = W/kT$ representing a dimensionless energy barrier for the formation of nuclei and S being the supersaturation ratio [16]. The pre-exponential term A represents the molecular kinetics of the formation of nuclei. According to the Szilard-Farkas model, the formation of nuclei is a stochastic process of consecutive attachment and detachment events of single molecules, yielding clusters of different sizes in the supersaturated solution [18]. The frequency of attachment of unit blocks to a nucleus (f^*) is assumed to be the rate limiting step of nucleus formation [19]. The precise assessment of f^* is challenging [16], yet our data provided evidence, that the ratio of the

attachment and detachment kinetics of precipitates, obtained from previously dissolved API through pH adaptation in the supersaturated phase was significantly higher for the IL as compared to the other groups tested (Fig. 4(c)). This suggested that the extended duration of supersaturation is at least in part driven by the counterion's impact on nucleus formation. This interpretation is supported by the linear dependency observed for the duration of supersaturation and the ratio of the counterion and the API (Fig. 4(f)). These solubility profiles obtained by potentiometric titration are determined using an accelerated method of measuring the duration of supersaturation and, therefore, real-time precipitation experiments were additionally performed (Fig. 3(c), (d)). In these real-time experiments, the potassium salt recrystallized within 12 min counteracting the positive effect of increased dissolution and questioning a sensible use *in vivo*. In contrast, the IL was stable in solution throughout 12 h (end of experiment), providing a more promising profile for further development. Nevertheless, more details are required to elucidate the broader impact of the IL, e.g. building off previous elegant studies detailing crystal growth dynamics of Theophylline by using crystal seeds [20]. In analogy, the impact of crystal growth on seeds prepared from the free acid can be profiled in solutions of the IL or the free acid.

Time lapsed diffractometric studies of the free acid and the IL detailed the crystalline status of precipitates formed in the supersaturated and the equilibrium phase generated from initially dissolved API by pH adaptation (Fig. 5(a), (b)). A faster collapse of the supersaturated phase was found for the free acid as compared to the IL, with precipitates from both groups being amorphous in the supersaturated phase and deprotonated at the sulfonamide group (Fig. 5(c)). The term amorphous is used in a sense that crystallinity was not detected based on interpretation of the diffractograms. However, we cannot exclude that other mesophases were present, which were not detected by XRPD [21]. Interestingly, the IL precipitated in the supersaturated phase together with the counterion (Fig. 5(c)), whereas the precipitate collected at equilibrium was composed of the free acid (Fig. 5(b)) indicating a different molecular association of the counterion and the API at supersaturated and equilibrium state, respectively. To elucidate the underlying mechanism, the API was further characterized in solution. The stable number and the chemical shifts of the signals measured by ^{1}H NMR at concentrations spanning from 0.125 to 4 mM (Supplementary Figure 4) and at 8 mM (Fig. 4(d)) suggested a concentration dependent formation of soluble associates, and the concentration effect on association was corroborated by mass spectrometry (data not shown). By ^{1}H NMR a striking change in peak intensity (and a signal shift) was observed at the supersaturated and equilibrium phase, respectively (Fig. 4(d)) as a result of precipitation and supported by the solubility measurements (Fig. 3(a), (b)). In contrast, this intensity change observed for

the API was not observed for the counterion. In conclusion, these experiments demonstrated that the counterion prolonged supersaturation by stabilizing the deprotonated state of the API. The moment the counterion fails in doing so, the API is precipitating as the free acid. This is further supported by the decrease of the API concentration with a stable concentration of the counterion in solution at equilibrium. Therefore, the mechanism is characterized by a constant increase of the counterion to API ratio in the supersaturated state as a result of the advancing precipitation of the API while the counterion does not precipitate (API precipitates as free acid; counterion remains in solution). This increase of the counterion to free acid ratio correlated to prolonged supersaturation (Fig. 4(f)) and, thereby, a self-stabilizing loop is closed leading to long-lasting supersaturation of the API. Furthermore, the IL may be formulated into a gastro-protective to prevent rapid collapse of the free acid in the gastric environment with high proton concentrations.

Solubility and / or permeability challenges are typically addressed by the synthesis of prodrugs, rapidly metabolizing entities leading to the parent drug already during or shortly after uptake. The acetylation of the sulfonamide group yielded a prodrug with a five times enhanced permeability through Caco-2 monolayers (Fig. 6(b)) but four times reduced solubility (Fig. 6(c)) as compared to the free acid. In contrast, the increased solubility of the IL, translated into an increased amount of absorbed substance as compared to the free acid or the prodrug. *In vivo* studies are needed to substantiate this first evidence for better bioavailability of the IL.

We conclude that the formation of an IL positively impacted the permeability through Caco-2 cell layers in terms of dissolution rate and time of supersaturation potentially widening the window for API uptake within the GIT.

Previous studies link the counterion to a skin irritation potential, however, the study was conducted with an irrelevant setup for the administration as profiled here within [22]. We performed initial cell viability studies of the counterion on kidney and liver cells as well as on macrophages and cell viability was affected in the upper μM or lower mM range, indicating a rather benign safety profile which must be substantiated by rigorous pre-clinical toxicology studies.

CONCLUSION

We detailed the mechanism of the favorable solubility profile of the IL as compared to the free acid, its potassium salt and the prodrug. The counterion of the IL had different effect on the API in the solid *versus* the liquid state. From the solid state, the dissolution was 700 fold faster in comparison to the free acid as a result of reduced lattice energy. Advantages in the liquid state of the IL resulted from increased solubility as well as from a constant increase of the counterion to API ratio with

time (counterion remained in solution, API precipitated in part), a mechanism which was demonstrated to increase supersaturation. Ultimately, both mechanisms resulted in an increased transepithelial transport *in vitro*. However, future *in vivo* studies are required to demonstrate whether these promising features of the IL translate into biopharmaceutical advantages.

MATERIALS AND METHODS

Materials

Dulbecco's MEM powder and Trypsin powder substance were purchased from Biochrome AG (Berlin, Germany) and Fetal Bovine Serum and RPMI medium from Gibco (Darmstadt, Germany). Caco-2 cells were purchased from DSMZ (Braunschweig, Germany). 4′, 6-diamino-2-phenylindole (DAPI) was purchased from Invitrogen (Carlsbad, CA) and Human E-Cadherin MAb (clone 180215) from R&D systems (Minneapolis, MN). Acetonitrile HPLC grade and potassium chloride (KCl) were purchased from VWR (Radnor, PA). Penicillin and streptomycin solution (Pen/Strep), non-essential amino acids (NEA), Hank's Balanced salts powder (without phenol red and sodium hydrogen carbonate), tetrabutylphosphonium hydroxide solution (40% in water v / v; referred to as 'counterion' within this manuscript), trifluoracetic acid (TFA), fluorescein sodium salt, hydrochloric acid 0.5 M, HEPES, glucose and acetic acid (≥99.7%) were purchased from Sigma Aldrich (St. Louis, MO). N-[7-Isopropyl-6-(2-methyl-2H-pyrazol-3-yl)-2,4-dioxo-1,4-dihydro-2H-quinazolin-3-yl]-methanesulfonamide (referred to as 'free acid' within this manuscript) and N-[7-isopropyl-6-(2-methyl-2H-pyrazol-3-yl)-2,4-dioxo-1,4-dihydro-2H-quinazolin-3-yl] N-methylsulfonyl-acetamide (referred to as 'prodrug' within this manuscript) were synthesized by Novartis AG (Basel, Switzerland) [7–9]. Sodium chloride, sodium hydrogen carbonate, sodium dihydrogen phosphate, disodium hydrogen phosphate, formaldehyde, ethanol and methanol were of analytical grade. Deuterated water (D_2O, 99.9% D) was purchased from Deutero GmbH (Kastellaun, Germany), deuterated water (D_2O, 99.9% D) containing 0.05% 3-(trimethylsilyl)propionic-2,2,3,3-d_4 acid-Na (TSP-d_4) from Sigma-Aldrich (Schnelldorf, Germany), hexadeuteriodimethyl sulfoxide (DMSO-d_6, 99.8% D) from Euriso-top (Saarbrücken, Germany), anhydrous dibasic sodium phosphate (99%) from Acros Organics (Geel, Belgium) and AVS Titrinorm 0.1 M hydrochloric acid and 0.1 M sodium hydroxide solution from VWR (Darmstadt, Germany). Standard 5 mm NMR tubes (ST 500) were purchased from Norell (Landisville, PA) and coaxial insert tubes from Wilmad-LabGlass (Vineland, NY). J774.1 cells, HepG2 cells and HEK 293 T cells were purchased from ATTC (Manassas, VA).

Methods

Ionic Liquid and Potassium Salt Preparation

The ionic liquid (IL) was prepared in analogy to previous reports [23]. Briefly, 1 g free acid was suspended in 40 mL acetone, an equimolar amount of the counterion (tetrabutylphosphonium hydroxide) was added and mixed until a clear solution was obtained. Solvents were evaporated at 40°C, 150–300 mbar until approximately 2 ml were left. The liquid was transferred onto a watch crystal and dried at 50°C *in vacuo* for 1 day. For the preparation of the potassium salt, 0.5 g acid was suspended in 5 ml ethanol in a round-bottomed flask. The resulting mixture was heated to 40°C and a solution of 0.083 g of potassium hydroxide in 0.5 ml of water was added continuously over 3 min. The solution was cooled to 20–25°C under stirring. Crystals were collected after 1 h by filtration with a filter crucible (pore size 4, Winzer, Wertheim, Germany). The filter cake was washed two times with 1 ml of ethanol and was dried at 50°C for 2 h *in vacuo* to yield 0.45 g salt.

High Performance Liquid Chromatography

Free acid, IL and prodrug samples were analyzed using a HPLC La Chrome Ultra equipped with a diode array detector L2455U, autosampler L-2200U and column oven L-2300 (Hitachi, Schaumburg, IL) on a Zorbax SB-C18 RRHT column (4.6×50mm, 1.8 µm; Agilent, Waldbronn, Germany) at a column temperature of 40°C. Mobile phase A was 0.1% TFA in water and mobile phase B was 0.1% TFA in acetonitrile with the gradient profile set as follows for mobile phase B: 0–3.5 min 15–65%; 3.5–3.7 min 65–15% and 3.7–5 min 15%. The flow rate was set at 1.2 mL/min and detection at $\lambda = 254$ nm.

Time Lapsed, Potentiometrically and Photometrically Recorded Titration Experiments for Determination Solubility, Duration of Supersaturation, Precipitation Rate, pka and Dissolution Rate

Intrinsic and kinetic solubility and the duration of the supersaturation were measured on a Sirius T3 instrument (Sirius Analytical, Forest Row, UK) by potentiometric titration as described before [12, 24]. In brief, typically 10 mg of API were dissolved in 1.5 ml of 0.15 M KCl solution at pH 12 (adjusted with 0.5 M potassium hydroxide). After complete dissolution, the solution was back-titrated by addition of 0.5 M hydrochloric acid until first precipitation occurred and as continuously monitored photometrically ($\lambda = 500$ nm). Subsequently, the pH was changed incrementally by repeated

addition of minute amounts of acid and base throughout the experiment. After each titrant addition the delayed pH gradient of the API due to precipitation or dissolution was measured and used to extrapolate the equilibrium phase where the pH gradient is zero. The duration of supersaturation is the time interval from the first precipitation (kinetic solubility) to the time when the concentration dropped below the kinetic solubility. Data from analysis with acidity errors larger than 1 mM were excluded. Precipitation and dissolution rates were recorded for the supersaturated and equilibrium phases, respectively. The precipitation rate was calculated as the change in molar concentration over time (dc/dt) after titration of minute amounts of hydrochloride acid (precipitation rate) or potassium hydroxide (dissolution rate), respectively. Concentration changes due to different titrant volume additions were corrected. pKa was determined on the Sirius T3 in potentiometric mode and according to the manufacturer's instruction. Besides by potentiometric titration, duration of supersaturation was determined by real time precipitation experiments with the Sirius T3 instrument. 8 µmol potassium salt and IL, respectively, were completely dissolved in 1.5 ml PBS pH 6.8 and pH was monitored over 1 h for potassium salt and 12 h for the IL. The change in pH due to precipitation was detected.

Dissolution rates were determined as described earlier [25]. Tablets with defined surface were prepared by compression of 5–10 mg substance in a tablet disc under a weight of 0.18 tonnes for 6 min with a manual hydraulic tablet press (Paul Weber Maschienen- und Apparatebau, Stuttgart-Uhlbach, Germany). Tableting is to render the dissolution rate independent of the surface, which was kept constant at 7.07 mm^2 throughout the experiment. Tablets were used for the experiment if these had a smooth surface. Visible cracks or other defects were not observed and solid particles did not detach from the tablet surface during the experiment. Dissolution rates were determined photometrically at room temperature in phosphate buffered saline (PBS) pH 6.8.

X-Ray Powder Diffractometry

Precipitates were collected from the solubility experiments after the first precipitation occurred and subject to X-ray powder diffractometry (XRPD) analysis. These suspensions were filtered through a paper filter (Macherey-Nagel MN 615, 7 cm diameter) using a filter crucible *in vacuo*. Precipitates as observed in the equilibrium phase were collected after stable intrinsic solubility concentration was recorded typically for 10 min. Powder diffractometric studies were done with a Bruker Discover D8 powder diffractometer (Karlsruhe, Germany) using Cu-Kα radiation (unsplit Kα$_1$+Kα$_2$ doublet, mean wavelength λ=154.19 pm) at a power of 40 kV and 40 mA, a focusing Goebel mirror and a 1.0 mm microfocus alignment (1.0 mm pinhole with 1.0 mm snout). Samples were prepared on a flat aluminum surface. Detection of the scattered X-ray beam went through a receiving slit with 7.5 mm opening, a 0.0125 mm nickel foil and a 2.5° axial Soller slit. Detection was done with a LynxEye-1D-Detector (Bruker AXS) using the full detector range of 192 channels. Measurements were done in reflection geometry in coupled two theta/theta mode with a step size of 0.025° in 2θ and 0.25 s measurement time per step in the range of 8–40° (2θ). Data collection and processing was done with the software packages DIFFRAC. Suite (V2 2.2.690, Bruker AXS 2009–2011, Karlsruhe, Germany) and DIFFRAC. EVA (Version 2.1, Bruker AXS 2012–2012, Karlsruhe, Germany). Simulation of the theoretic pattern of the free acid was done from the cif-file obtained from single crystal analysis with the program Mercury (Mercury 3.1 Development – Build RC5, CCDC 2001–2012, Cambridge, UK).

Differential Scanning Calorimetry and Thermogravimetry

Differential Scanning Calorimetry (DSC) was performed on a DSC 8000 instrument (Perkin Elmer, Waltham, MA) using a scanning rate of 20 K/min. Sample size was 2.10, 5.52, 0.85 and 1.67 mg for the free acid, the IL, the potassium salt and the prodrug, respectively. For the IL, the second heating cycle was analyzed to allow removal of residual water during the first heating cycle. Crucibles were weighed before and after measurements. A Q5000 TGA (TA instruments, New Castle, DE) was used for thermo gravimetric analysis. The platinum crucible was tarred first and then loaded with substance. The scan rate was 10°C / min from 30 to 300°C.

Nuclear Magnetic Resonance Measurement

NMR measurements were performed on a Bruker Avance 400 MHz spectrometer (Karlsruhe, Germany) operating at 400.13 MHz with a BBO BB-H 5 mm probe head, and data processing with the TopSpin 3.0 software. The temperature was adjusted with a BCU-05 (Bruker) temperature control unit. Solid-state ^{15}N VACP/MAS NMR spectra were recorded at 22°C on a Bruker DSX-400 NMR spectrometer with bottom-layer rotors of ZrO$_2$ (diameter 7 mm) containing approximately 200 mg of sample. A resonance frequency of ^{15}N 40.6 MHz, referenced to external standard glycine (^{15}N, δ=−342.0) was set with a spinning rate of 6.8–7 kHz, contact time 3 milliseconds, 90° transmitter pulse length of 3.6 microseconds and a repetition time of 4 s. 2120 scans were collected for the potassium salt and the free acid and 20,000 scans were collected for the IL. For pKa assignment and characterization of the precipitates by ^{1}H NMR measurements the following acquisition parameters were applied: 16 scans, at a temperature of 300 K, flip angle of 30°, spectral width of 20.55 ppm, and transmitter offset of 6.175 ppm. The acquisition time was set to 3.985 s followed by a relaxation delay of 1.0 s with collection of 64 K data points at a sample spinning frequency

of 20 Hz. Processing parameters were set to an exponential line broadening window function of 0.3 Hz, an automatic baseline correction and manual phasing. For the aggregation assay based on concentration dependent ^{1}H NMR signal shift measurements, 256 scans were collected at a temperature of 300 K using otherwise identical parameters as described above. The spectra were referenced to the external standard of 0.05% sodium trimethylsilylpropionate in D_2O (TSP-d_4) filled in a coaxial insert tube. For sample preparation of the pKa assignment experiment, four samples of 9 mg free acid each were suspended in 10 ml Millipore water. The pH was adapted to 3.57, 5.57, 7.61, and 11.75, respectively, using either 0.1 M aqueous hydrochloric acid or 0.1 M aqueous potassium hydroxide. The samples were lyophilized for 24 h (Christ Lyophilisator Alpha 1–4 LD plus; Osterode, Germany) and dried samples were dissolved in 700 µl DMSO-d_6 before measurement. The sample preparation for the concentration range / aggregation assay was as described before with modification [14]. Briefly, 7.64 mg IL were weighted into a 2 mL Eppendorf tube and dissolved in 1500 µL buffer (8 mM sample; 200 mM dibasic sodium phosphate buffer in D_2O pH 7.4 (pD 7.8). 500 µL of this stock solution was immediately transferred into a 1.5 mL Eppendorf tube and another 500 µL buffer were added yielding a 4 mM solution, and vigorously shaken for 2 min. This dilution step was repeated in order to establish a dilution series of 0.125, 0.25, 0.5, 1, 2, 4, and 8 mM. The 8 mM sample was measured from supernatants collected from the supersaturation and in the equilibrium phase, respectively.

Infrared Spectroscopy

The measurements were conducted on Jasco FT/IR-6100 spectrometer from Jasco (Gross-Umstadt, Germany) with diamond attenuated total reflection unit.

Single Crystal Diffraction

Single crystals of the free acid were obtained by recrystallization of the product in methanol with access to benzene. The recrystallization of the potassium salt was performed by dissolving 2 mg in 1 mL acetontrile with two drops of methanol and evaporating the solvent. Suitable single crystals were mixed with high viscosity perfluorinated polyalkylether (99.9%, ABCR, 1800 cSt). Selected crystals were mounted and fixed on a plastic quill and instantly cooled in a gas stream of dry, evaporating liquid nitrogen. Data collection for the free acid was performed on a X-ray single crystal diffractometer based on a BRUKER D8 3-axis goniometer with a CCD SMART APEX I detector system (Bruker AXS Inc., Madison, WI) with standard graphite monochromator using sealed tube Mo-Kα radiation (unsplit Kα$_1$ λ= 70.93 pm Å + Kα$_2$ λ=71.35 pm doublet, mean λ=

71.073 pm) at a power of 40 kV and 40 mA at a temperature of 168 K [3]. Operation software was the SMART Suite Software package (v 5.0 Bruker AXS Inc.). Frame acquisition strategy consisted of 2124 frames (512×512 pixels, acquisition time 20 s) in 6 runs with ω (0°, 60°, 120°, 180°, 240°, 300°) and a range of 180° Φ (0.5° steps) for each run. Data collection for the potassium salt was performed on a X-ray single crystal diffractometer based on a BRUKER FR591 κ-goniometer with a CCD APEX II detector system (Bruker AXS Inc.) with Helios multilayer mirror monochromator using rotating anode Mo-Kα radiation (unsplit Kα$_1$ λ=70.93 pm Å + Kα$_2$ λ= 71.35 pm doublet, mean λ=71.073 pm) at a power of 50 kV and 40 mA at 100 K [2]. Operation software is the Apex II Suite Software package (v 2012.4-3, Bruker AXS Inc.). Frame acquisition strategy consisted of 1320 frames (512×512 pixels, acquisition time 30 s) in 9 runs covering the complete Laue sphere. Both datasets were processed with the Apex II Suite Software package (v 2012.4–3, Bruker AXS Inc.) including the SAINT+ Integration Engine (v 8.18C, Bruker AXS Inc.) for data integration, the SADABS software (v 2008/1, Bruker AXS, Inc.) for absorption correction, XPREP v 2008/2, Bruker AXS Inc.) for the preparation of instruction files and reflection lists. Structure solution via direct methods and structure refinement was made with SHELXS [26] and SHELXL [26] from the software package SHELXTL (v 6.14 8/06/00 Bruker AXS Inc.). Integrity of symmetry was checked with PLATON (v 1.16) [27]). GUIs used for refinement and extraction of crystallographic data are X-SEED (v 2.05) [28] and OLEX 2 (v 1.2) [29]. For all species, all non-hydrogen atoms were refined anisotropically and all hydrogen atoms were refined isotropically on their specified atomic positions by least square methods.

Mass Spectrometry

The experiments were conducted as described before with modification [13]. Three solutions of the IL were prepared in Nanopure water: acetonitrile mixtures at a volume ratio of 7:3 and 3:7, respectively, yielding a final concentration of the IL of 1 mmol/L. Samples were directly injected into the an Agilent (Palo Alto, CA) 1100 Series LC/MSD Trap system via ESI-interface with a syringe pump Model 100 (KD scientific, Holliston, MA) at a flow rate of 1 ml/h. The liquid stream was nebulized with nitrogen gas at a flow of 5 L/min and a nebulizer pressure of 15.0 psi. The analysis was done by means of the LC/MSD Trap version 5.3 software (Agilent, Waldbronn, Germany). An ESI ionization method in a negative mode and a scan range from 200 to 4000 m/z was used. The drying gas temperature was set to 110°C so that associated molecules of the IL could be transferred into the gas phase. The overall goal was to conserve intermolecular interaction throughout analysis as described before [30].

In Vitro Permeability Through the Caco-2 Cell Monolayer Model

Cells were grown in Dulbecco's modified Eagle's medium high glucose (DMEM) with penicillin and streptomycin (Pen/Strep) as described before [31, 32]. In brief, 500 mL medium were prepared with Dulbecco's modified eagle medium (DMEM) powder containing 4.5 g glucose, 50 mL Fetal Bovine Serum, 5 mL 100× nonessential amino acids (NEA) and 5 mL Pen/Strep (penicillin 10,000 U/mL and streptomycin 10 mg mL^{-1} solution 100×). Caco-2 cells were cultured at 37°C and 5% CO_2 in cell culture medium. 2.7×10^5 cells / cm^2 (counted with Neubauer improved hemocytometer; LO-Laboroptik, Friedrichsdorf, Germany) were seeded on polycarbonate filter inserts (diameter 12 mm; 0.4 µm membrane pore size) on 12 well plates (Corning life science, Amsterdam, The Netherlands). Cells typically had 54–56 passages. The monolayer integrity was monitored by measuring the transepithelial electrical resistance (TEER) and fluorescein added to the apical compartment as a leakage marker. TEER measurements were performed for each cell-seeded filter using a chopstick electrode EVOM2 STX3 electrode and EVOM2 epithelial voltammeter (World Precision Instruments, Sarasota, FL). Specifications for cell-seeded filters required TEER values exceeding 600 (Ω*cm^2) [15, 31, 33]. Sodium fluorescein was applied to two filters of each 12 well plate, following previously published protocols [15, 33]. In brief, 20 µM sodium fluorescein Hank's Buffered Salt Solution (HBSS) buffer solution were applied apically. Samples for reading the fluorescence were taken at all-time points when samples were collected for the API transport study and analyzed on 96 well plates (96 F nontreated white microwell SH; Nunc, Penfield, NY) with a LS50B fluorescence spectrometer (Perkin Elmer, Waltham, MA). The apparent permeability coefficients (P_{app}; cm/sec) were calculated as follows: $P_{app} = (dQ/dt)(1/A*C_o)$ and dQ/dt being the steady-state flux [µmol/sec], A being the insert/filter surface area [cm^2] and c_0 being the starting concentration in the apical (donor) chamber [µM]. Transport studies were performed as described before and typically commencing 21–23 days after seeding of the cells on the inserts [32, 34]. For that, HBSS buffer (pH 7.4) was used for sample preparation and as the basolateral (receiving) medium. The APIs were applied apically either as a solution with a concentration of 0.26 mM for the free acid, 0.26 mM for the IL or 0.056 mM for the prodrug (maximal prodrug concentrations after 3 h in solution (0.13 mM at pH 7.4) were lower as those for the IL (2.74 mM at pH 7.4) and the free acid (0.68 mM at pH 7.4) due to solubility limitation). Basolateral API amounts from acid and IL solution experiments were normalized in order to compensate for the higher apical concentrations of acid and IL in comparison to prodrug. Another transport study explored the APIs applied as suspensions to the apical (donor) compartment. For that, suspensions were prepared in 400 µl of HBSS buffer for each filter insert,

holding amounts of 1.47 ± 0.08 µmol for the free acid, 1.55 ± 0.05 µmol for the IL or 1.33 ± 0.05 µmol for the prodrug ($n \geq 5$ filter inserts per group). Samples were typically collected from the basolateral (uptake) compartment after 30 min. Sodium fluorescein samples were analyzed by fluorescence spectroscopy. The monolayers were further characterized after completion of the transport studies by cell nuclei stain and in representative filters for e-cadherine (cell contacts) labeling. For that, cells on the filters were exposed to 4% formaldehyde in PBS pH 7.4 for 20 min and filters were treated with 0.1% Triton X in PBS pH 7.4 for 10 min and exposed to 5% BSA in PBS pH 7.4 buffer for 60 min, thereafter. Mouse antibody against human e-cadherin was diluted 1:100 in PBS pH 7.4 and applied for 2 h at room temperature after which a secondary antimouse Alexa Fluor 488 antibody (Life Technologies, Darmstadt, Germany; diluted 1:200 in blocking solution) was applied and subjected to the confocal microscopy, thereafter. Cell nuclei were labeled with 4′,6-diamidine-2-phenylindol (DAPI) and diluted 1:1000 in PBS pH 7.4 according to the manufacturer's protocol and subjected to the confocal microscopy (Leica TCS-SP2, Wetzlar, Germany; lens 63/1.4 oil), thereafter.

Cytotoxicity of Counterion

Tetrabutlyphosphonium chloride was dissolved and serially diluted in DMSO. For the experiments J774.1 and HepG2 cells were suspended at a concentration 1×10^5 cells/ml in RPMI medium with 10% FCS and without phenol red. HEK 293 T cells were diluted to 2×10^4 cells/ml in DMEM high glucose medium with 10% FCS and without phenol red. 200 µl of cell suspensions were transferred into 96-well cell culture plates and the API dilutions were added. The final concentration of DMSO was 1%. After 24 h of incubation at 37°C and 5% CO_2, 10% of AlamarBlue solution were admixed. J774.1 and HepG2 cells were incubated for further 48 h and HEK 293 T cells for 24 h. The IC_{50} values were calculated, with respect to controls without APIs, from the absorbance values measured at 550 nm, using 630 nm as reference wavelength.

REFERENCES

1. Miller DA, Watts AB, Williams III RO. Formulating poorly water soluble drugs. New York: Springer; 2012.

2. Lipinski CA, Lombardo F, Dominy BW, Feeney PJ. Experimental and computational approaches to estimate solubility and permeability in drug discovery and development settings. Adv Drug Deliver Rev. 1997;23:3–25.

3. Johnson KE. What's an ionic liquid? Electrochem Soc Interface. 2007;16:38–41.

4. D.R. MacFarlane, J.M. Pringle, K.M. Johansson, S.A. Forsyth, and M. Forsyth. Lewis base ionic liquids. Chem Commun (Camb):1905–1917 (2006).

5. Hough WL, Smiglak M, Rodriguez H, Swatloski RP, Spear SK, Daly DT, *et al.* The third evolution of ionic liquids: active pharmaceutical ingredients. New J Chem. 2007;31:1429–36.

6. Stellaand VJ, Nti-Addae KW. Prodrug strategies to overcome poor water solubility. Adv Drug Delivery Rev. 2007;59:677–94.

7. Russo E, Gitto R, Citraro R, Chimirri A, De SG. New AMPA antagonists in epilepsy. Expert Opin Invest Drugs. 2012;21:1371–89.

8. Orain D, Ofner S, Koller M, Carcache DA, Froestl W, Allgeier H, *et al.* 6-Amino quinazolinedione sulfonamides as orally active competitive AMPA receptor antagonists. Bioorg Med Chem Lett. 2012;22:996–9.

9. Koller M, Lingenhoehl K, Schmutz M, Vranesic I-T, Kallen J, Auberson YP, *et al.* Quinazolinedione sulfonamides: a novel class of competitive AMPA receptor antagonists with oral activity. Bioorg Med Chem Lett. 2011;21:3358–61.

10. B. Gomez-Mancilla, R. Brand, T.P. Jurgens, H. Gobel, C. Sommer, A. Straube, S. Evers, M. Sommer, V. Campos, H.O. Kalkman, S. Hariry, N. Pezous, D. Johns, and H.-C. Diener. Randomized, multicenter trial to assess the efficacy, safety and tolerability of a single dose of a novel AMPA receptor antagonist BGG492 for the treatment of acute migraine attacks. Cephalalgia (2013).

11. Ahmed R, Gogal M, Walsh JE. A new rapid and simple nonradioactive assay to monitor and determine the proliferation of lymphocytes: an alternative to [3H]thymidine incorporation assay. J Immunol Methods. 1994;170:211–24.

12. Hsieh Y-L, Ilevbare GA, Van EB, Box KJ, Sanchez-Felix MV, Taylor LS. pH-induced precipitation behavior of weakly basic compounds: determination of extent and duration of supersaturation using potentiometric titration and correlation to solid state properties. Pharm Res. 2012;29:2738–53.

13. Dorbritz S, Ruth W, Kragl U. Investigation on aggregate formation of ionic liquids. Adv Synth Catal. 2005;347:1273–9.

14. LaPlante SR, Carson R, Gillard J, Aubry N, Coulombe R, Bordeleau S, *et al.* Compound aggregation in drug discovery: implementing a practical NMR assay for medicinal chemists. J Med Chem. 2013;56:5142–50.

15. Imai T, Sakai M, Ohtake H, Azuma H, Otagiri M. In vitro and in vivo evaluation of the enhancing activity of glycyrrhizin on the intestinal absorption of drugs. Pharm Res. 1999;16:80–6.

16. Davey RJ, Schroeder SL, ter Horst JH. Nucleation of organic crystals—a molecular perspective. Angew Chem Int Ed Engl. 2013;52:2166–79.

17. M. Volmerand Editor. Die chemische Reaktion. Bd. IV. Kinetik der Phasenbildung, J. W. Edwards (1939).

18. Kashchiev D, van Rosmalem GM. Review: nucleation in solutions revisited. Cryst Res Technol. 2003;38:555–74.

19. Sangwal K. Nucleation: basic theory with applications edited by dimo kashchiev. Cryst Res Technol. 2001;36:235.

20. Rodriguez-Hornedo N, Lechuga-Ballesteros D, Wu HJ. Phase transition and heterogeneous/epitaxial nucleation of hydrated and anhydrous theophylline crystals. Int J Pharm. 1992;85:149–62.

21. Stevenson CL, Bennett DB, Lechuga-Ballesteros D. Pharmaceutical liquid crystals: the relevance of partially ordered systems. J Pharm Sci. 2005;94:1861–80.

22. Dunn BJ, Nichols CW, Gad SC. Acute dermal toxicity of two quaternary organophosphonium salts in the rabbit. Toxicology. 1982;24:245–50.

23. Bica K, Rijksen C, Nieuwenhuyzen M, Rogers RD. In search of pure liquid salt forms of aspirin: ionic liquid approaches with acetylsalicylic acid and salicylic acid. Phys Chem Chem Phys. 2010;12:2011–7.

24. Stuartand M, Box K. Chasing equilibrium: measuring the intrinsic solubility of weak acids and bases. Anal Chem. 2005;77:983–90.

25. Gravestock T, Box K, Comer J, Frake E, Judge S, Ruiz R. The "GI dissolution" method: a low volume, in vitro apparatus for assessing the dissolution/precipitation behaviour of an active pharmaceutical ingredient under biorelevant conditions. Anal Methods. 2011;3:560–7.

26. Sheldrick GM. A short history of SHELX. Acta crystallographica section A. Foundations of crystallography. 2008;64:112–22.

27. Spek AL. Structure validation in chemical crystallography. Acta crystallographica section D. Biological crystallography. 2009;65:148–55.

28. Barbour LJ. X-seed - a software tool for supramolecular crystallography. J Supramol Chem. 2003;1:189–91.

29. Dolomanov OV, Bourhis LJ, Gildea RJ, Howard JAK, Puschmann H. OLEX2: a complete structure solution, refinement and analysis program. J Appl Cryst. 2009;4:339–41.

30. Gozzo FC, Santos LS, Augusti R, Consorti CS, Dupont J, Eberlin MN. Gaseous supramolecules of imidazolium ionic liquids: "Magic" numbers and intrinsic strengths of hydrogen bonds. Chem Eur J. 2004;10:6187–93.

31. Jager H, Meinel L, Dietz B, Lapke C, Bauer R, Merkle HP, *et al.* Transport of alkamides from Echinacea species through Caco-2 monolayers. Planta Med. 2002;68:469–71.

32. Hubatsch I, Ragnarsson EG, Artursson P. Determination of drug permeability and prediction of drug absorption in Caco-2 monolayers. Nat Protoc. 2007;2:2111–9.

33. Masungi C, Borremans C, Willems B, Mensch J, Van Dijck A, Augustijns P, *et al.* Usefulness of a novel Caco-2 cell perfusion system. I. In vitro prediction of the absorption potential of passively diffused compounds. J Pharm Sci. 2004;93:2507–21.

34. Hakala K, Laitinen L, Kuakonen AM, Hirvonen J, Kostiainen R, Kotiaho T. Development of fast LC/MS/MS methods for cocktail dosed Caco-2 samples using atmospheric pressure photoionization (APPI) and electrospray ionization (ESI). Eur J Pharm Sci. 2003;19:S30–30.